sustainability

MDPI

Article

Mechanical Properties, Self-Healing Characteristics, and Chloride-Ion Penetration Resistance of Cement-Free Composites Incorporating Aluminosilicate Material-Based Capsules

Se-Jin Choi [1], Jeong-Yeon Park [1], Chunho Chang [2] and Jae-In Lee [1,*]

[1] Department of Architectural Engineering, Wonkwang University, 460 Iksan-daero, Iksan 54538, Republic of Korea; csj2378@wku.ac.kr (S.-J.C.); jkite7490@naver.com (J.-Y.P.)
[2] Department of Civil Engineering, Keimyung University, Daegu 42601, Republic of Korea; chunho@kmu.ac.kr
* Correspondence: jaein0482@daum.net

Abstract

The construction sector is currently tasked with the critical challenge of minimizing CO_2 emissions associated with cement manufacturing. To support a sustainable building environment, this research developed cement-free alkali-activated composites by leveraging industrial by-products, specifically fly ash and blast furnace slag. The study experimentally evaluated how aluminosilicate material-based capsules (AMCs) composed of a mixture of fly ash, blast furnace slag, and ferronickel slag powder affect the composites' durability, mechanical properties, and self-healing capabilities, alongside microstructural investigations. Results indicated that specimens incorporating 10% AMC reached a compressive-strength recovery range of 112–118%, which represents an improvement of approximately 10% compared to the control sample. Furthermore, the 28-day resistance to chloride ion penetration was enhanced by 79.4%, successfully meeting the 'very low' permeability criteria defined by ASTM C 1202. These results suggest that cement-free self-healing composites incorporating AMCs are a viable alternative for reducing carbon emissions and minimizing environmental impact in the construction industry. Furthermore, the recycling of industrial byproducts, as demonstrated herein, contributes to sustainable development in response to climate change.

Keywords: cement-free; aluminosilicate materials; self-healing; blast furnace slag; fly ash; ferronickel slag; capsule

Check for updates

Academic Editors: Hyunjin Ju and Sun-Jin Han

Received: 6 January 2026
Revised: 6 February 2026
Accepted: 27 February 2026
Published: 2 March 2026

Copyright: © 2026 by the authors. Licensee MDPI, Basel, Switzerland. This article is an open access article distributed under the terms and conditions of the Creative Commons Attribution (CC BY) license.

1. Introduction

Concrete possesses high compressive strength and durability [1]. Cement, which is used as a binder in concrete, is an essential material in the construction industry [2]. Global greenhouse gas emissions are significantly impacted by cement production, which accounts for roughly 7–8% of the world's total due to its high energy consumption and massive CO_2 release [3,4].

The construction industry faces the urgent challenge of reducing carbon dioxide emissions from cement production. Consequently, recent research has focused on cement-free composites that utilize various industrial byproducts as binders instead of cement [5–7]. Cement-free composites using binders, such as blast furnace slag powder and fly ash, are known to reduce carbon dioxide emissions by up to 80% compared with ordinary cement concrete [8]. Because these binders lack the ability to react with water independently, the addition of an alkali activator is essential to trigger the hydration-like process [9]. Moreover,

since the durability and mechanical strength of cement-free composites are highly sensitive to the specific proportions and types of alkali activators and binders, meticulous material selection is required [10].

Cement-free composites have a higher performance than conventional cement-based concrete in terms of compressive strength, acid resistance, and shrinkage [11]. Consequently, they have attracted attention as potential replacements for cementitious concretes [12]. The research by You et al. [13] focused on how different dosages and types of activators affect the microstructure and mechanical properties of fly ash-based geopolymers. They demonstrated that using calcium sulfate and calcium hydroxide provides the necessary Ca^{2+} ions to facilitate fly ash crystal dissolution and the subsequent formation of gel products. Klerk et al. [14] investigated the effect of adding industrial waste powders to fly ash-based geopolymers. They reported that while the addition of waste marble powder alone led to performance deterioration, the combined use of waste bottom ash and waste ceramic powder resulted in improved performance. Hao et al. [15] evaluated the effect of biochar incorporation on ground granulated blast furnace slag (GGBS)-based geopolymer composites. They reported that the incorporation of 1 wt% biochar resulted in the best performance; however, biochar addition exceeding 10 wt% led to a degradation in mechanical properties. Cai et al. [16] found that increasing GGBS content in ultra-high-performance geopolymer concrete leads to higher elastic modulus and compressive strength. Similarly, another study by Cai et al. [17] noted that a higher GGBS ratio improves matrix density, benefiting the overall compressive strength of fly ash/GGBS-based composites. Regarding long-term properties, Gomes et al. [18] observed that while increasing blast furnace slag powder enhances carbonation resistance, it also tends to increase drying shrinkage in geopolymers.

However, cement-free composites have been reported to be relatively more brittle and have lower fracture energies than conventional cement-based concrete, making them vulnerable to crack propagation [19,20]. When cracks occur in cement-free composites, carbon dioxide and harmful elements can penetrate through the cracks, causing problems such as reinforcement corrosion and structural degradations and potentially reducing the stability of these composites [21].

Recent studies have been conducted on self-healing cement-free composites to mitigate the issue of reduced durability. Ekinci et al. [22] evaluated the effects of *Bacillus subtilis* on a blast furnace slag-based geopolymer paste. The evaluation showed that specimens containing bacteria exhibited higher durability and better mechanical properties than those without bacteria, attributed to their metabolic activity.

Harun et al. [23] investigated the mechanical properties of metakaolin-based geopolymers introduced with bacteria. They reported that when bacteria were added by the injection method, cracks in the geopolymer specimens were most effectively sealed, and the flexural strength recovery rate was the highest. Hammad et al. [24] examined the effects of the concentration of *Bacillus subtilis* on the mechanical properties and durability of alkali-activated slag composites. The incorporation of *Bacillus subtilis* resulted in superior compressive and flexural strengths. Luhar et al. [25] evaluated the influence of *Sporosarcina pasteurii* on metakaolin-based geopolymer concrete, noting that the bacteria promoted the formation of $CaCO_3$, which subsequently filled the cracks. In a study on the self-healing of fly ash/slag-based geopolymers, Zhao et al. [26] reported that exposure to a $Ca(OH)_2$ solution yielded the most effective healing results by promoting $CaCO_3$ precipitation. Additionally, Ozen et al. [27] conducted an evaluation of the self-healing capabilities of geopolymer composites that integrated sodium silicate-based capsules. The results showed that the specimens cured under high-temperature conditions of 60 °C and 100% relative humidity exhibited the most effective healing performance.

Ulugol et al. [28] examined how blast furnace slag powder influences the self-healing of geopolymer composites made from construction and demolition waste (CDW). Their results indicated that $CaCO_3$ formation is the primary mechanism for healing, and this effect is further amplified by the inclusion of slag powder. Although various studies are underway to mitigate the durability degradation issues in cement-free composites, such as by utilizing bacteria and industrial byproducts, research applying encapsulated aluminosilicate materials to cement-free composites remains limited.

Biological self-healing methods utilizing bacteria have attracted considerable attention. However, they are limited by high culture costs and low microbial survival rates in the highly alkaline environment of cement-free composites. In contrast, aluminosilicate material-based capsules (AMCs) offer a simpler manufacturing process compared with bacteria-based approaches, making them more cost-effective. Furthermore, by directly utilizing industrial byproducts, they offer an alternative that enhances resource recycling and sustainability. Nevertheless, research on directly applying these capsules to cement-free composites to elucidate their mechanisms remains scarce.

Alkali-activated composites incorporating self-healing capabilities through AMC can effectively overcome the limitations of conventional repair methods in the construction industry, such as surface treatment and injection methods. Conventional methods require manual intervention, such as applying sealants or high-pressure injection (epoxy injection), once cracks are detected. These processes demand skilled labor and involve complex procedures, leading to significant repair durations. In contrast, the AMC allows the healing agents within the capsules to react immediately with moisture upon crack formation, enabling autonomous crack repair. This approach minimizes the need for additional maintenance personnel, thereby reducing labor costs. Furthermore, it significantly shortens the repair wait times and construction periods, which is expected to maximize maintenance efficiency and economic viability of structures.

Therefore, this study investigated the effects of AMCs, such as blast furnace slag powder, fly ash, and ferronickel slag powder, on the mechanical properties, chloride ion penetration resistance, self-healing properties, and microstructure of cement-free composites. The aim was to reduce the carbon footprint of the construction industry and contribute to a sustainable construction environment by introducing self-healing capsules into cement-free composites.

2. Materials and Methods

2.1. Materials

Following a previous study [5], we employed blast furnace slag powder and fly ash as the primary binders. To activate these binders, CaO, $Ca(HCOO)_2$, $Ca(NO_3)_2$, and NaOH were incorporated as alkali activators in powder form, serving as binder replacements. Natural sand (NS), with a fineness modulus of 2.45 and a density of 2.60 g/cm^3, was used as the fine aggregate.

To optimize the self-healing efficiency, AMC particles were prepared by mixing two size ranges, 0.3–0.6 mm and 2.5–5.0 mm, in a 5:5 ratio. This mixed distribution has been reported to exhibit superior performance to single-size capsules [29]. The aluminosilicate materials constituting the capsules comprised blast furnace slag powder, fly ash, and ferronickel slag powder (POSCO, Pohang-si, Republic of Korea). The composition ratio of the materials used for capsule fabrication was determined through preliminary experiments. The optimal ratio, under which the cohesion and mechanical performance were optimized, was selected for this study. Polyvinyl alcohol (PVA; Amos, Hwaseong-si, Republic of Korea) was added to improve the cohesion between the materials during the encapsulation process. In addition, a polyurethane solution (KCC, Seoul-si, Republic of Korea) was

applied as a protective coating during the mixing stage to ensure structural stability of the capsules and prevent premature rupture. The coating process was repeated three times to obtain a uniform thickness, and the final coating was dried for 24 h to induce complete polymerization of the coating layer. Tables 1 and 2 present the chemical properties of the aluminosilicate materials and the properties of the alkali activators used in this study, respectively. Table 3 lists the physical properties of the fine aggregates; Table 4 presents the material composition ratios based on the AMC type. Figure 1 shows the aluminosilicate materials used in this study. Figures 2 and 3 show the morphology and SEM images of NS and AMC, respectively. As shown in the figures, AMC exhibits a relatively rounder shape than NS.

Table 1. Chemical composition of the binders used in this study.

Type	SiO_2	Al_2O_3	Fe_2O_3	CaO	MgO	K_2O	Blaine (cm^2/g)	Density (g/cm^3)
Blast furnace slag powder (BS)	30.6	13.9	0.32	40.7	6.4	0.6	4210	2.93
Fly ash (FA)	64.88	20.56	6.06	2.58	0.80	1.45	3710	2.21
Ferronickel slag powder (FS)	48.8	2.8	13.7	1.1	30.6	-	15,890	3.09

Table 2. Physical properties of the alkali activator.

Type	pH	Density (g/cm^3)	After Ignition (%)	Manufacturer
CaO	-	3.3	97.5	Daejung (Siheung-si, Republic of Korea
$Ca(HCOO)_2$	7.31	1.9	99.4	
$Ca(NO_3)_2$	6.0	1.9	98.8	
NaOH	-	2.13	99.1	

Table 3. Physical properties of the fine aggregate.

Material	FM	Density (g/cm^3)	Water Absorption (%)
NS	2.45	2.60	1.0

Table 4. Composition ratio of AMC samples (unit: %).

Type	BS	FA	FS
F-FS	-	50	50
B-FS	50	-	50
B-FF	60	20	20



(**a**) (**b**) (**c**)

Figure 1. Aluminosilicate materials used in this study: (**a**) BS, (**b**) FA, and (**c**) FS.

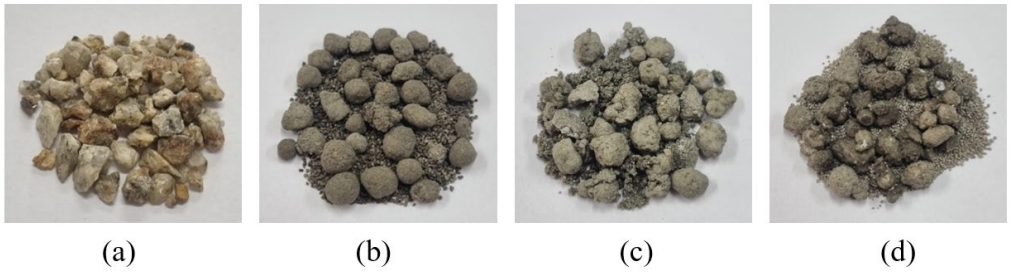


Figure 2. Aggregates used in this study: (**a**) NS, (**b**) F-FS, (**c**) B-FS, and (**d**) B-FF.

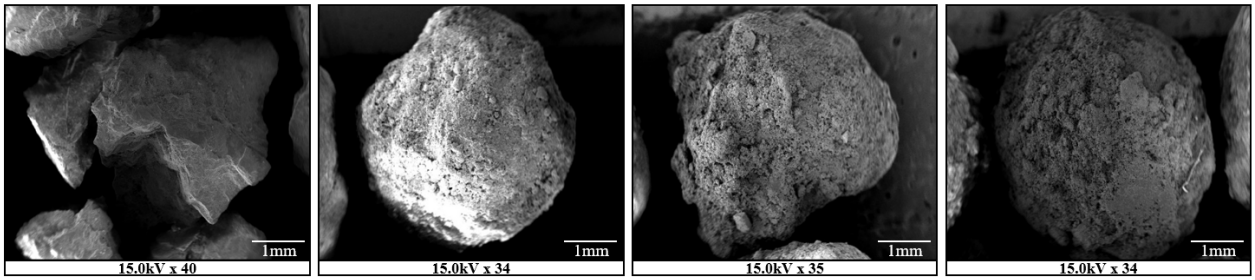


Figure 3. SEM images of (**a**) NS, (**b**) F-FS, (**c**) B-FS, and (**d**) B-FF.

2.2. Mixing Proportions and Specimen Preparation

Table 5 presents the mixing proportions of the mortar samples. The water–binder ratio (W/B) was fixed at 40%, and the AMC was blended at 0%, 5%, and 10% by weight of fine aggregate.

Table 5. Mixing proportions of mortar samples.

Type	AMC (g)	Sand (g)	Water (g)	BS (g)	FA (g)	CaO (g)	$Ca(NO_3)_2$ (g)	$Ca(HCOO)_2$ (g)	NaOH (g)
Cube									
50 mm × 50 mm × 50 mm	0	4496							
Cylindrical	225	4272	1013	1899	253	63	126	126	63
Ø50 mm × 100 mm	450	4047							
Ø100 mm × 50 mm									

To investigate the mechanical properties and durability of AMC-incorporated cement-free composites, several types of specimens were prepared. Specifically, 50 mm × 50 mm × 50 mm cubic specimens were molded for assessing the compressive strength and recovery rate. For tensile strength evaluation, Ø50 mm × 100 mm cylinders were employed, while Ø100 mm × 50 mm cylindrical samples were utilized to analyze crack reduction and chloride ion penetration resistance. For the microstructural analysis, pieces were collected from the center of the specimen to measure the 28-day compressive strength; the analysis was conducted using scanning electron microscopy (SEM; AIS1800C, Seron, Republic of Korea) and energy-dispersive X-ray spectroscopy (EDS; Oxford Instrument, Xplore, High Wycombe, UK).

The specimens were demolded 24 h after fabrication and steam-cured in a steam-curing chamber maintained at 40 °C and 100% relative humidity until the required curing age.

To evaluate the properties of cement-free composites containing AMC, the mortar fluidity and compressive strength were measured in accordance with the KS L 5105 standard [30]. To evaluate the self-healing performance, the compressive strength recovery rate was measured using the following procedure: First, the reference compressive strength

was determined at 28 days of age. Subsequently, a pre-load equivalent to 70% of the reference compressive strength was applied to the recovery test specimens at the same age to induce micro-cracks under a constant loading rate of 2.5 kN/s. After the loading process, the specimens were re-cured for a specified period, and the compressive strength was measured upon reaching the target healing age. The compressive strength recovery rate was calculated as a percentage, representing the ratio of the healed strength relative to the reference compressive strength. Furthermore, the splitting tensile strength was evaluated in accordance with the KS F 2423 guidelines [31], and the chloride ion penetration resistance was rigorously assessed using the method specified in ASTM C 1202 [32]. To evaluate the self-healing performance, crack widths were measured at the same locations based on the curing period using an optical microscope (GB-959, Global4You, Seongnam-si, Republic of Korea; magnification range of 20× to 800×) and digital vernier calipers (SD500-150PRO, SINCON, Bucheon-si, Republic of Korea; accuracy of ±0.03 mm). At 28 days of age, the specimens were split, and silicon sheets were inserted to induce cracks. Subsequently, the cracks were fixed using clamps, and the specimens were re-cured. The changes in the crack width were then measured based on the healing age. The compressive strength, compressive strength recovery rate, and splitting tensile strength were measured using a universal testing machine (CHUNKWANG PREC. INS. IND, Hanam-si, Republic of Korea) with a maximum capacity of 100 t. For the chloride ion penetration resistance, measurements were conducted for 12 h under an applied voltage of 30 V using a chloride ion penetration and diffusion coefficient tester (Daeyoon Scale Industry, Seoul-si, Republic of Korea).

Scanning electron microscopy combined with energy-dispersive X-ray spectroscopy (SEM-EDS) was employed for the microstructure analysis at an accelerating voltage of 15 kV.

3. Results and Discussion

3.1. Mortar Flow

Figure 4 shows the change in the mortar flow of the cement-free composites mixed with AMC. The control sample showed the lowest flow of approximately 186 mm among all the samples. For the AMC-incorporated sample, the flow was approximately 189–198 mm, similar to or relatively higher than that of the control sample. This result is attributed to the relatively rounder shape of the AMC particles compared with NS, as observed in Figure 3. Furthermore, the sample with 10% AMC admixture exhibited a relatively higher flow rate than that with 5% AMC admixture.

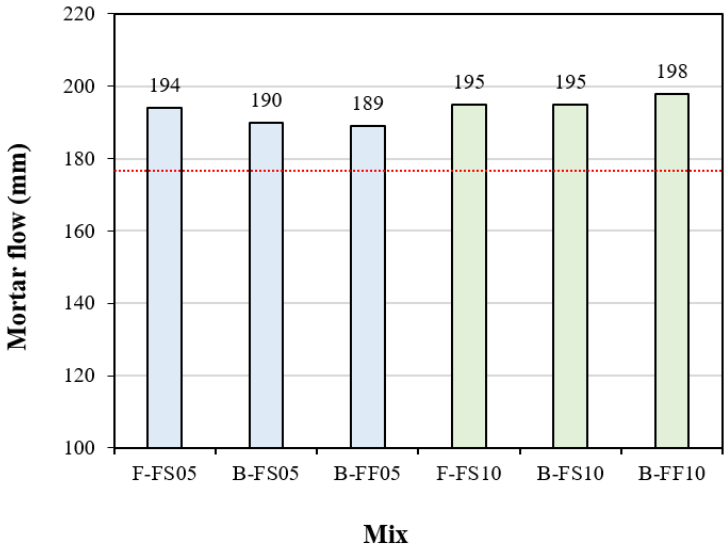


Figure 4. Mortar flow in cement-free composites mixed with AMC (Red dotted line: Control).

3.2. Compressive Strength

The temporal evolution of the compressive strength of the AMC-incorporated cement-free composites is illustrated in Figure 5. At the early stage of 7 days, the control group achieved a compressive strength of approximately 19.4 MPa. Regarding the samples incorporating 5% AMC, samples F-FS05 and B-FS05 exhibited compressive strengths of 21.5–25.9 MPa, representing levels 10.8–33.5% higher than that of the control sample. Sample B-FF05 exhibited a compressive strength of approximately 17.2 MPa, which was the lowest among the samples containing 5% AMC.

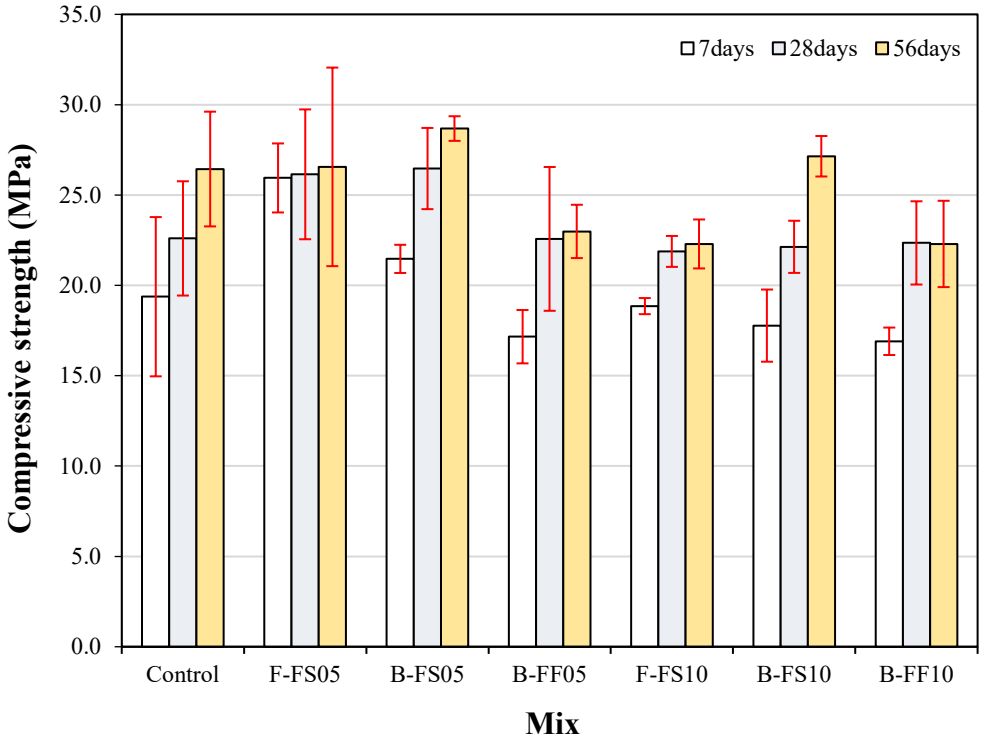


Figure 5. Compressive strength of AMC-incorporated cement-free composites.

The tendency of some of the AMC-blended samples to exhibit a relatively higher compressive strength than the control sample could be attributed to potential damage to some of the capsules during mixing. This damage caused material decomposition of the capsules, thereby increasing the unit binder content. Meanwhile, the sample with 10% AMC showed compressive strengths in the range of 16.9–18.9 MPa, indicating a relatively lower level compared with the control sample.

Regarding the compressive strength at 7 days, for the same capsule type, the compressive strength tended to decrease with increasing AMC blending rate. This trend probably resulted from AMC having a relatively rounder shape than NS, which affected its bonding strength with the matrix [33], and from the increase in the number of microvoids as the capsules blended [34].

After 28 days of curing, the control sample exhibited a compressive strength of approximately 22.6 MPa. Similar to the 7-day trend, samples F-FS05 and B-FS05 showed compressive strengths of 26.1–26.5 MPa, representing levels approximately 15.5–17.3% higher than that of the control sample.

B-FS05 exhibited the highest compressive strength, approximately 26.5 MPa. This was attributed to microvoid filling due to the high reactivity of the fine blast furnace slag powder that constituted the capsules destroyed during mixing and the high fineness of the

ferronickel slag fine powder [35]. B-FF05 exhibited a compressive strength of approximately 22.6 MPa, which was similar to that of the control sample.

For specimens with 10% AMC, the measured strengths ranged from 21.9 to 22.4 MPa. Similar to the 7-day compressive strength, the compressive strength showed an inverse relationship with the amount of AMC added; however, these values remained similar to those of the control sample (22.6 MPa).

At 56 days, the strength of the control sample was approximately 26.4 MPa. Similar to the 28-day compressive strength results, the B-FS05 sample exhibited the best mechanical performance, recording the highest strength of approximately 28.7 MPa. The F-FS05 sample exhibited a strength of 26.6 MPa, similar to the control, while the B-FS10 sample exhibited the best performance among the 10% AMC mixtures, recording a strength of 27.1 MPa. The F-FS10 and B-FF10 samples recorded similar values of approximately 22.3 MPa.

3.3. Splitting Tensile Strength

Figure 6 shows the tensile strength of cement-free composites containing AMC after 28 days. The control specimen recorded the lowest tensile strength of approximately 2.0 MPa among all samples.

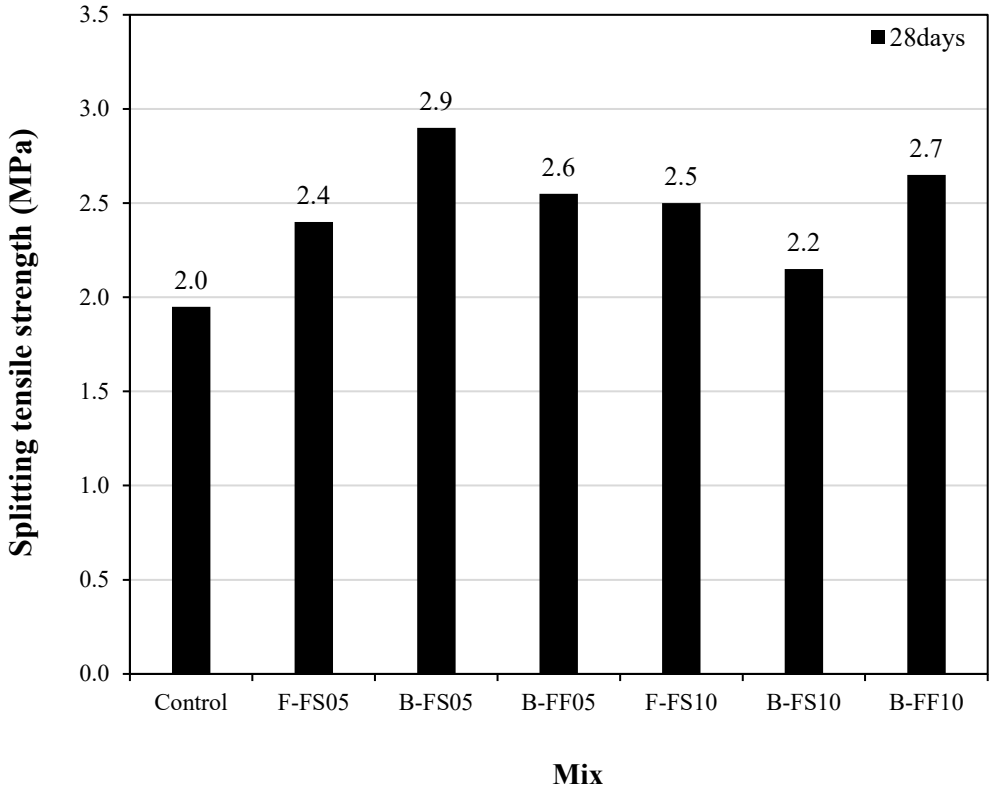


Figure 6. Splitting tensile strength of AMC-incorporated cement-free composites.

Conversely, specimens containing 5% AMC showed significant improvement, with tensile strengths ranging from 2.4 to 2.9 MPa. This represents a 9.1% to 31.8% increase compared with the control. In particular, the B-FS05 specimen achieved a maximum tensile strength of approximately 2.9 MPa. This result is consistent with the 28-day compressive strength results, demonstrating similar mechanical behavior under various loading conditions. Among the specimens containing 10% AMC, the B-FS10 specimen exhibited the lowest tensile strength of approximately 2.2 MPa. B-FS capsules exhibited an angular surface morphology (Figure 3), which enhanced the bonding strength with the matrix. Consequently, under compressive loading, specimens incorporating these capsules demonstrated improved strength compared to those with relatively spherical capsules. However,

when subjected to splitting tensile loads, the sharp edges of the capsules may act as stress concentration points. These points potentially serve as initiation sites for crack propagation, leading to the observed reduction in the tensile strength [36]. F-FS10 and B-FF10 samples exhibited similar tensile performance, with measured values ranging from 2.5 to 2.7 MPa.

Overall, in terms of tensile strength, all the AMC-blended samples exhibited relatively higher tensile strength than the control sample, generally showing a trend similar to the 28-day compressive strength. These results suggest that, although the rounded particle shape of AMCs may slightly reduce the compressive strength during incorporation, some of the AMCs may be damaged during mixing. The materials that decomposed from the damaged AMCs then react continuously, leading to the observed high tensile strength.

3.4. Chloride-Ion Penetrability

Figure 7 shows the chloride-ion penetration resistance of cement-free composites containing AMC at different ages. The control sample aged for 28 days showed the highest total charge among all the samples, approximately 1676 C.

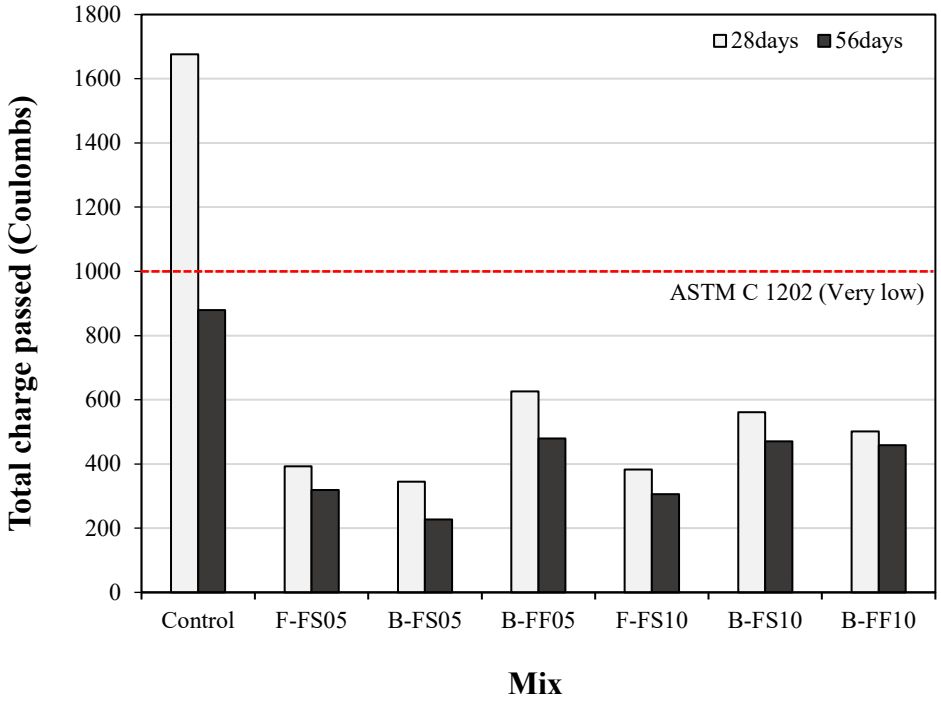


Figure 7. Chloride-ion penetrability of AMC-incorporated cement-free composites.

The AMC-incorporated samples showed a total charge ranging from approximately 345 to 626 C, regardless of the AMC type or incorporation rate, representing levels 62.6–79.4% lower than that of the control sample. B-FS05 exhibited the lowest level at approximately 345 C among all samples. This result was attributed to the relatively dense internal structure formed owing to the highest compressive strength observed after 28 days of aging [37].

Furthermore, for chloride-ion permeability resistance at 28 days of curing, all the AMC-incorporated samples, except for the control sample, exhibited values corresponding to "very low" as specified in ASTM C 1202. This result indicates that the incorporation of AMC positively influenced the chloride ion permeability resistance of the cement-free composite.

At 56 days of aging, the control sample exhibited the highest total charge of approximately 879 C among all the samples, whereas B-FS05 showed the lowest charge, approximately 227 C, similar to the trend observed at 28 days.

Regardless of the AMC mixing ratio, the F-FS and B-FF samples exhibited total charges of approximately 306–319 and 459–479 C, respectively, which were 65.2% lower than those of the control sample.

3.5. Compressive Strength Recovery Rate

Figure 8 shows the results of the self-healing efficiency evaluation, expressed in terms of the compressive strength recovery rates for various curing periods. At the initial 7-day point, the control sample achieved a recovery of approximately 92%. In comparison, samples containing 5% AMC exhibited recovery rates ranging from approximately 85% to 93%, demonstrating similar or slightly lower performance than the control sample.

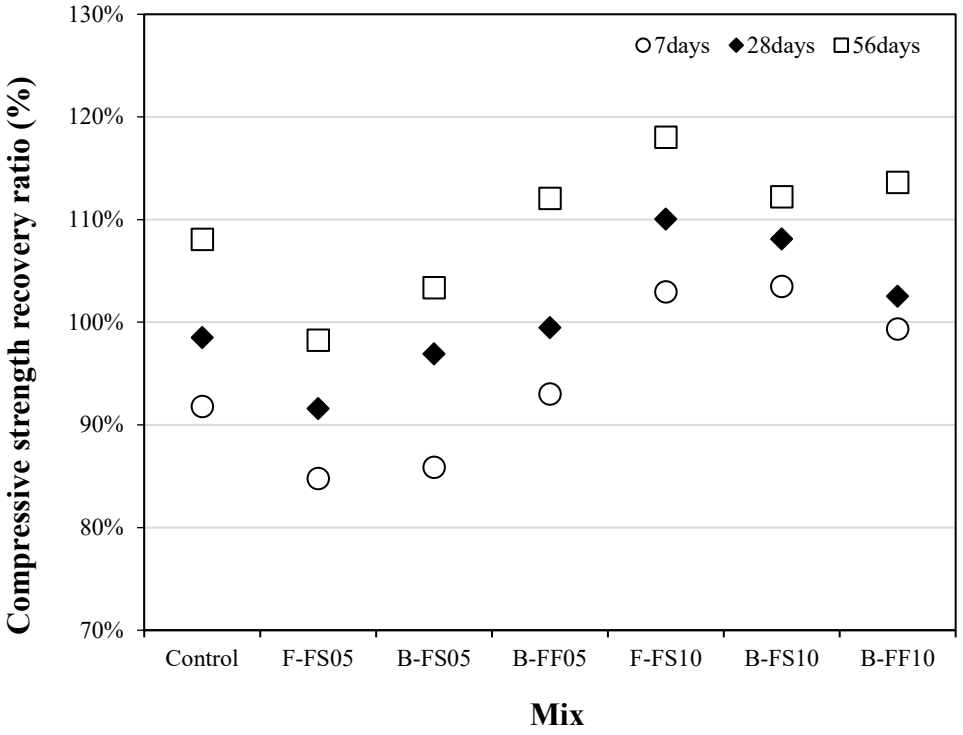


Figure 8. Compressive strength recovery rate of AMC-incorporated cement-free composites.

Samples containing 10% AMC exhibited recovery rates ranging from 99% to 103%, demonstrating a significant improvement of 7% to 11% compared with the control sample. In particular, the F-FS10 and B-FS10 samples exhibited the highest recovery rates (approximately 103%) among all samples, suggesting that higher capsule contents (10% compared to 5%) were more effective in recovering initial strength.

After 28 days of curing, the control sample achieved a recovery rate of approximately 99%, while the 5% AMC samples (B-FS05 and B-FF05) maintained similar recovery rates, ranging from approximately 97% to 99%. However, the 10% AMC samples consistently performed well, with the F-FS10 and B-FS10 samples achieving excellent recovery rates of approximately 108% to 110%, approximately 16% to 18% higher than that of the control sample.

At the 56-day long-term curing stage, the control sample achieved a recovery rate of approximately 108%. The 5% AMC specimens (F-FS05 and B-FS05) lagged slightly behind at approximately 103%; however, the F-FS10 sample consistently maintained excellent performance, achieving approximately 118%. With the exception of a few specific samples, most of the AMC-containing cement-free composites demonstrated improved long-term recovery rates compared with the control sample. This superior performance is primarily attributed to the reaction of decomposed materials within the aluminosilicate-

based capsules over time. This process promotes sustained hydration, positively impacting the long-term structural densification and self-healing capacity of the cement-free composite matrix.

3.6. Reduction of Crack Size

Figure 9 shows the temporal evolution of crack size reduction in cement-free composites containing AMC over the re-curing period. At 7 days, the control sample showed a minimum crack reduction efficiency of approximately 5%. In contrast, specimens containing AMC showed reduction rates ranging from 8% to 12%, demonstrating a 3% to 7% improvement over the control sample. In particular, the B-FF10 sample demonstrated the highest initial healing rate, achieving a 12% reduction rate.

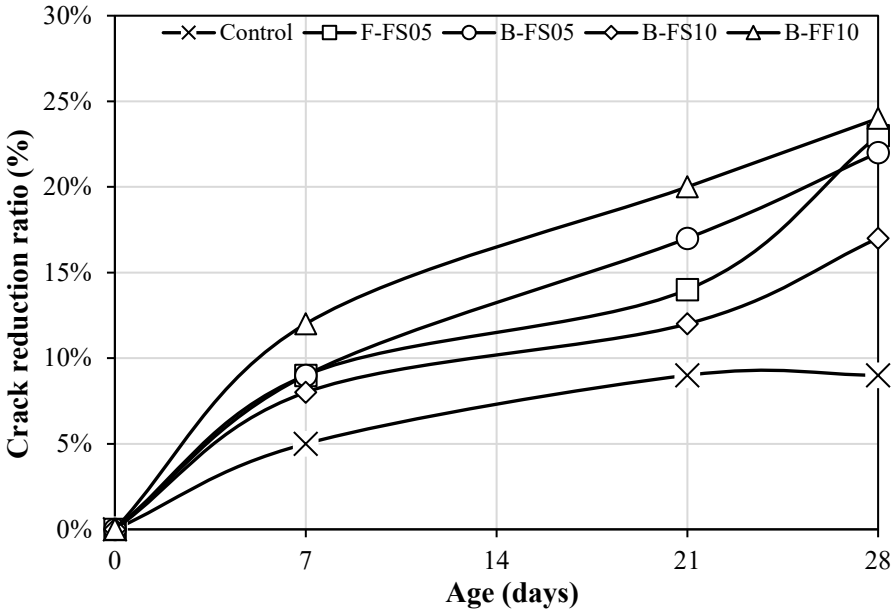


Figure 9. Reduction of crack size in cement-free composites containing AMC.

After 21 days of re-curing, the crack reduction rate of the control sample remained relatively stable at around 9%, similar to that at 14 days. However, specimens containing AMC showed sustained and significant healing progress, with reduction rates increasing to a range of 12–20%. Among these, the B-FF10 variant maintained excellent performance, achieving a maximum crack reduction rate of approximately 20%, which was 11% higher than that of the control sample.

At the final 28-day observation point, the crack reduction rate of the control sample plateaued at 9%, and no further improvement was observed after 2 weeks. In contrast, the specimens containing 5% AMC (F-FS05 and B-FS05) exhibited strong self-healing ability with a final reduction rate of 22% to 23%, which was 13% to 14% higher than that of the control sample. Within the group containing 10% AMC, B-FS10 showed the lowest efficiency of 17% among the capsule-containing samples; however, it still showed an 8% higher reduction rate than the control sample, confirming that the presence of AMC significantly promoted the physical closure of microcracks within the cement-free matrix. Furthermore, B-FF10 showed the highest crack reduction rate of approximately 24% among all the samples. This trend probably resulted from microcracks being filled because of the high reactivity of the blast furnace slag powder and fly ash decomposed in AMC and the hydration reaction of the ferronickel slag powder at long-term ages [38].

Figure 10 shows the crack changes in the specimens immediately after cracking and after 28 days of re-curing. For the B-FF10 sample, which exhibited the highest crack-healing

rate, significant internal healing was observed. For the F-FS05 and B-FS05 samples, which showed similar crack-reduction rates, filling of the internal cracks by the healing agent was also observed. In particular, B-FS05 showed complete crack sealing, demonstrating the best crack-sealing effect among all the samples. However, the measured crack reduction rate was lower than that of B-FF10 because the crack reduction rate was calculated by measuring the surface size of the formed cracks. After 28 days of re-curing, internal cracks were clearly visible on the crack surface of the control sample (without AMC). Similar phenomena were observed in the B-FS10 sample, which showed the lowest crack reduction rate among the samples with AMC.

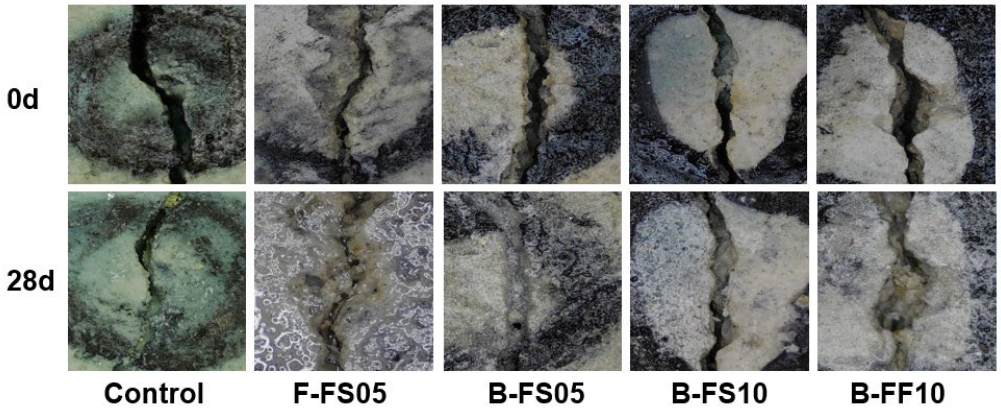


Figure 10. Crack size change in cement-free composites containing AMC.

3.7. Microstructural Analysis

Figure 11 shows SEM images of the specimens at 28 days. B-FS05, which achieved the highest compressive strength at 28 days, exhibited a dense matrix with relatively few cracks and voids. Unreacted fly ash particles were observed in F-FS05, in which fly ash and ferronickel slag fines were used as encapsulating materials. Furthermore, the control and B-FF05 specimens exhibited similar compressive strengths (approximately 22.6 MPa) at 28 days, indicating minimal differences in the SEM images.

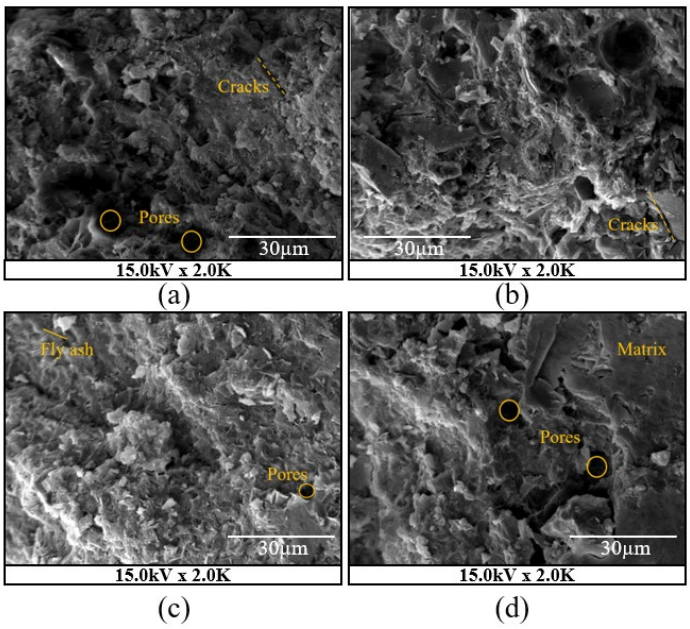


Figure 11. SEM image of 28 d specimen (2000×): (**a**) Control, (**b**) F-FS05, (**c**) B-FS05, and (**d**) B-FF05.

Table 6 and Figure 12 present the EDS analysis results for the 28-day compressive strength recovery test of the control and B-FF05 samples. The elements constituting the control and B-FF05 samples, including Ca, Al, Si, and K, were similar. However, the control sample showed a higher content of some elements than the B-FF05 sample, and the Ca content, which contributed to the strength development, differed by approximately 7.1%.

Table 6. EDS spot results for C-(A)-S-H in the control and B-FF05 samples (wt.%).

Mix	Ca	Al	Si	K	Si/Al
Control	54.9	4.2	10.1	0.4	2.39
B-FF05	47.8	2.0	4.5	0.6	2.29

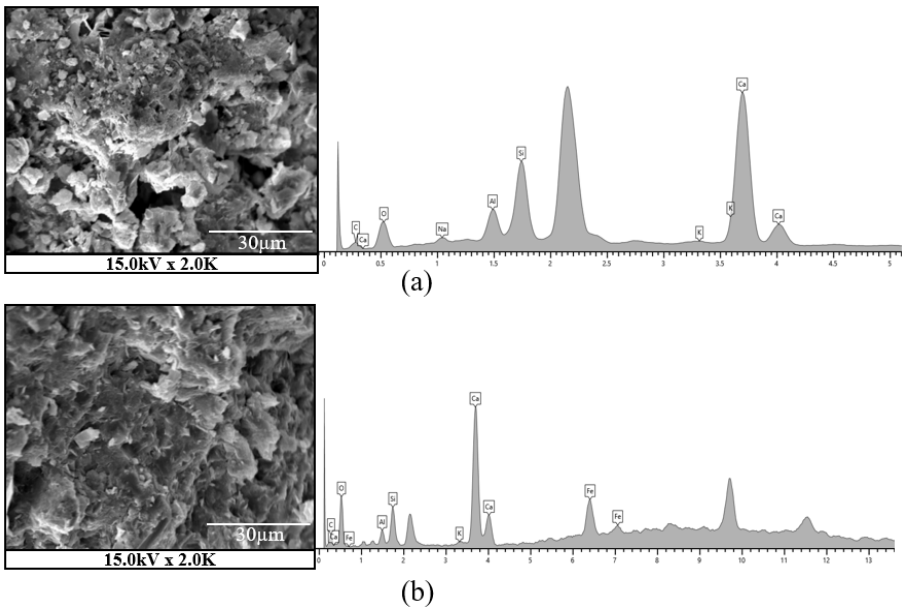


Figure 12. EDS spot results of 28 d specimen (2000×): (**a**) Control and (**b**) B-FF05.

The lower Ca content of the B-FF05 sample may be attributed to its aluminosilicate material content. When the capsule is fractured under a load, the materials constituting the capsule decompose and react during the re-curing period. At this time, the capsule components, such as the blast furnace slag powder and fly ash, do not directly react with water but instead consume $Ca(OH)_2$ [39], which is believed to be the reason for the relatively low Ca content.

Furthermore, the Si/Al ratios of the two samples, calculated using the elemental content, ranged from 2.29 to 2.39, showing no significant difference. This result is likely due to the similar compressive strength recovery rates of approximately 99% after 28 days of curing for both samples. Furthermore, the aluminosilicate material in the B-FF sample formed a hydrate similar to that in the control sample, that is, a C-(A)-S-H gel composed of Ca, Al, and Si. The Si/Al ratio is used to determine the stability of the resulting gel [40,41], and a high Si/Al ratio has been reported to contribute to microstructural stabilization and improved mechanical performance [41].

4. Discussion

We performed a comparative performance analysis of the AMC-integrated cement-free composites investigated in this study with cement-free and self-healing composites reported in the literature, as listed in Table 7.

Table 7. Performance summary of cement-free composites in terms of AMC incorporation and comparison with existing studies.

Sample	Chloride Ion Penetration (Coulombs)	Splitting Tensile Strength (MPa)	Compressive Strength (MPa)	28 Days Crack Recovery Ratio (%)	Ref.
Control	1676	2.0	22.6	9	Current study
F-FS05	393	2.4	26.1	23	
F-FS10	383	2.5	21.9		
B-FS05	345	2.9	26.5	22	
B-FS10	561	2.2	22.1	17	
B-FF05	626	2.6	22.6		
B-FF10	502	2.7	22.4	24	
Control	3253		46.4		[24]
Bacteria cell/mL (10^3)			53.8		
Bacteria cell/mL (10^5)	1080		69.4		
Bacteria cell/mL (10^7)			55.1		
Geopolymer			49.7		[42]
MgO 4%			53.8		
MgO 6%			55.9		
MgO 8%			58.2		
MgO 12%			52.7		
Waterglass 5%			41.2		[43]
Waterglass 10%			60.7		
Waterglass 15%					
Waterglass 20%			80.5		
Control			43.4		[44]
Rice husk 5%			46.7		
Rice husk 15%			47.5		
Rice husk 20%					
Control	1800				[45]
Rice husk 5%	1500				
Rice husk 10%	1000				
Rice husk 15%	1200				
Rice husk 20%	1400				

As indicated in the table, previous studies related to cement-free composites have primarily focused on strength development, often utilizing high-concentration alkali activators or specific mineral additives (MgO and rice husk ash) to achieve high strength. In contrast, the AMC-integrated cement-free composites developed in this study exhibited superior durability within a practical strength range of 20–30 MPa by utilizing industrial by-products (BFS and FA) as binders. Notably, while existing research has frequently employed bacteria to achieve self-healing properties in cement-free systems, to the best of the authors' knowledge, no prior study has simultaneously evaluated the mechanical performance and durability of cement-free self-healing composites incorporated with AMC.

From Table 7, it is clear that the chloride ion penetration resistance of the AMC-integrated composites is superior to previously reported values. Their mechanical properties, including the compressive and splitting tensile strengths, also demonstrated improvements compared with those of the control sample. Consequently, while prior literature emphasized strength development, this study confirms that it is possible to maintain a practical strength of 20–30 MPa—suitable for general structures—while ensuring exceptional chloride ion penetration resistance and mechanical performance. These results suggest that the AMC-integrated cement-free composite can significantly contribute to achieving the dual goals of reducing carbon emissions and enhancing structural durability in the construction industry.

5. Conclusions

The development of environmentally friendly and sustainable construction strategies is imperative to mitigate carbon emissions in response to the climate crisis, particularly given that the construction industry accounts for approximately 8% of global carbon emis-

sions. This study focused on the development of cement-free composites to significantly reduce the carbon footprint associated with conventional cement production.

The incorporation of AMCs, which utilize industrial by-products, not only promotes resource circularity but also preserves natural aggregates and reduces the CO_2 emissions generated during aggregate extraction. Furthermore, the integration of self-healing technology minimizes the socio-economic and environmental costs required for maintenance, thereby enhancing the long-term sustainability of infrastructure.

In this research, a comprehensive analysis of the fluidity, mechanical properties, chloride-ion penetration resistance, self-healing performance, and microstructure of AMC-integrated cement-free composites was conducted. The key findings are as follows:

1. The mortar flow of the samples containing AMC was higher than that of the control sample, which is believed to be due to the rounded shape of the AMC particles.
2. The compressive strengths of the samples containing AMC decreased slightly with increasing AMC content. This result suggests that the shape of the AMC affects the bonding strength with the matrix of the cement-free composite. Furthermore, among the samples containing 5% AMC, the B-FS05 sample, which contained both fine blast furnace slag powder and fine ferronickel slag powder, exhibited the highest compressive strength. The B-FS10 sample exhibited the highest compressive strength when 10% AMC was used.
3. All the samples containing AMC exhibited higher tensile strengths than the control sample.
4. The 28-day passing charge of the samples containing AMC was approximately 79.4% lower than that of the control sample, demonstrating a significantly improved chloride ion penetration resistance. At all ages, the samples exhibited values corresponding to the "very low" standard defined by ASTM C 1202.
5. The compressive-strength recovery rate did not differ significantly from that of the control sample when 5% AMC was used. However, the compressive strength recovery rate of the samples containing 10% AMC was 112–118%, which was approximately 10% higher than that of the control sample.
6. The crack reduction rate evaluation results showed that all samples containing AMC exhibited higher crack reduction rates than the control sample. Even after 28 days, the control sample did not heal fully, whereas the samples containing AMC exhibited relatively high levels of healing.

The evaluation of the mechanical properties, durability, and self-healing performance of cement-free composites incorporating AMCs demonstrated that AMC-integrated samples achieved superior fluidity, compressive strength, and durability compared with the control. Furthermore, the mechanical recovery and crack reduction rates were significantly higher, confirming the potential of the self-healing technology for sustainable infrastructure maintenance by extending its service life.

However, some of the capsules might have been damaged during the mixing process due to physical impact, which could have influenced various performance aspects. Therefore, future research should focus on conducting a quantitative assessment of the capsule survival rate and developing a coating layer with enhanced strength to withstand high mixing energy. Such follow-up studies will be crucial for improving the practical field applicability of cement-free self-healing composites and ensuring the reliability of sustainable construction materials.

https://doi.org/10.3390/su18052425

Author Contributions: Conceptualization, S.-J.C.; Investigation, S.-J.C., J.-Y.P. and J.-I.L.; Data Curation, J.-Y.P., C.C. and J.-I.L.; Writing—Original Draft Preparation, S.-J.C. and J.-I.L.; Writing—Review and Editing, S.-J.C. and C.C. All authors have read and agreed to the published version of the manuscript.

Funding: This research was supported by a grant from the National Research Foundation of Korea (NRF) funded by the Korea government (MIST) (RS-2024-00405537).

Institutional Review Board Statement: Not applicable.

Informed Consent Statement: Not applicable.

Data Availability Statement: The original contributions presented in this study are included in the article. Further inquiries can be directed to the corresponding author.

Conflicts of Interest: The authors declare no conflicts of interest.

References

1. Lee, J.I.; Choi, S.J. Compressive strrength, chloride-ion-oenetration resistance, and crack-recovery properties of self-healing cement compoistes containing cementitious material capsules and blast-furnace-slag aggregates. *J. CO2 Util.* **2024**, *86*, 102916. [CrossRef]
2. Lee, J.I.; Kim, C.Y.; Yoon, J.H.; Choi, S.J. Mechanical properties of cement mortar containing ground waste newspaper as cementitous material. *Materials* **2023**, *16*, 1374.
3. Teshome, H.M. Using Bio-Based Self-Healing Agent for Durability and Environmentally Friendly Concrete Development. *Int. J. Concr. Struct. Mater.* **2025**, *19*, 102. [CrossRef]
4. Marandi, N.; Shirzad, S. Sustainalbe cement and concrete technologies: A review of materials and processes for carbon reduction. *Innov. Infrastruct. Solut.* **2025**, *10*, 408. [CrossRef]
5. Lee, J.I.; Kim, C.Y.; Yoon, J.H.; Lee, H.J.; Choi, S.J. Effect of curing method on the mechanical properties and durability of blast furnace slag based geopolymer composite containing ferronickel slag powder. *J. Korea Concr. Inst.* **2024**, *36*, 297–307. [CrossRef]
6. Maaze, M.R.; Das, S.K.; Garg, N.; Shrivastava, S. Economic-Environmental and Multi-Criteria Optimization for Predicting Alkaline Ratios in Waste Cement Concrete-Based Geopolymer Using Central Composite Design. *Int. J. Concr. Struct. Mater.* **2025**, *19*, 35. [CrossRef]
7. Amer, I.; Abdelkhalik, A.; Mayhoub, O.A.; Kohail, M. Development of Sustainable Slag-based Geopolymer Concrete Uisng Different Types of Chemical Admixtures. *Int. J. Concr. Struct. Mater.* **2024**, *18*, 27. [CrossRef]
8. Amer, I.; Kohail, M.; El-Feky, M.S.; Rashad, A.; Khalaf, M.A. Realistic evaluation of reinforcement bond strength in alkali-activated slag concrete exposed to elevated temperatures. *Int. J. Concr. Strruct. Mater.* **2023**, *17*, 36. [CrossRef]
9. Jagadisha, H.M.; Pandit, P.; Prashant, S.; Bhole, L.; Singh, Y.; Verma, O.; Kumar, M. Multi-objected Optimisation of One-Part Slag-Flyash-Microsilica Based Alkali-Activated Ternary Binder Mixes. *Int. J. Concr. Struct. Mater.* **2025**, *19*, 75. [CrossRef]
10. Rashad, A.M. A Concise on the Effect of Calcium Oxide on the Properties of Alkali-Activated Materials: A Manual for Civil Engineers. *Int. J. Concr. Struct. Mater.* **2023**, *17*, 72. [CrossRef]
11. Ng, C.; Alengaran, U.J.; Wong, L.S.; Kim, H.M.; Jumaat, M.Z.; Ramesh, S. A review on microstructural study and compressive strength of geopolymers mortar, paste and concrete. *Constr. Build. Mater.* **2018**, *186*, 550–576. [CrossRef]
12. Mohamed, O.A.; Hassan, A.; Abdelwahab, N.R. High-Performance and Durable Green Geopolymer Based on Slag/Alumina Sludge Ash Incorporating $CuFe_2O_4$ Spinel Nanograins for Enhanced Gamma Radiation Shielding. *Int. J. Concr. Struct. Mater.* **2025**, *19*, 87. [CrossRef]
13. You, J.; Ji, F.; Lv, Q.; Li, W.; Lin, Z.; Peng, Y. Mechanical property and microstructure of fly ash-based geoplymer by calcium activators. *Case Stud. Constr. Mater.* **2024**, *21*, e03811.
14. Klerk, D.D.; Naghizadeh, A.; Ekolu, S.O.; Purchase, M.W. Recycled cement use to produce fly ash-based geopolymer binders suitable for ambient curing: Comparison with slag effects. *Constr. Build. Mater.* **2025**, *468*, 140394. [CrossRef]
15. Hao, D.X.; Guo, Y.C.; Chen, R.; Zhou, L.; Han, Y.M. Mechanical and Microstructural Regulation of Biochar-Geopolymer composites from Industrial Slag Wastes. *Dev. Built Environ.* **2026**, *25*, 100862. [CrossRef]
16. Cai, Y.H.; Huang, T.; Huang, B.Y.; Hua, C.B.; Huang, Q.; Chen, J.W.; Liu, H.L.; He, Z.J.; Rouzi, N.B.; Xie, Z.H.; et al. Investigation into the Static Mechanical Properties of Ultra-High-Performance Geopolymer Concrete Incorporating Steel Slag, Ground Granulated Blast-Furnace Slag, and Fly Ash. *Buildings* **2025**, *15*, 2535. [CrossRef]
17. Cai, X.; Yin, J.; Xu, X.; Zhang, D.; Wang, Y. Rheological, mechanical, and microstructural properties of engineered geopolymer composite (EGC) made with ground granulated blast furnace slag (GGBFS) and fly ash. *J. Mater. Res. Technol.* **2025**, *35*, 1996–2010. [CrossRef]

18. Gomes, S.D.C.; Nguyen, Q.D.; Li, W.; Castel, A. Shrinkage and carbonation of alkali-activated calcined clay-ground granulated blast furnace slag (GGBFS) concrete. *Cem. Concr. Res.* **2025**, *194*, 107899. [CrossRef]
19. Alshaaer, M. Synthesis and characterization of self-healing geopolymer composite. *Constr. Build. Mater.* **2020**, *245*, 118432. [CrossRef]
20. Garces, J.I.Y.; Dollent, I.J.; Beltran, A.B.; Tan, R.R.; Promentilla, M.A.B. Life cycle assessment of self-healing geopolyemr concrete. *Celan. Eng. Technol.* **2021**, *4*, 100147.
21. Xian, J.; Qiu, J.; Wu, P.; Zhang, Q.; Song, Y.; Yang, L. Autolytic capsuels incorporating alkali-activated slag system for self-healing cementitous composites. *Cem. Concr. Compos.* **2024**, *147*, 105439. [CrossRef]
22. Ekinci, E.; Turkmen, I.; Birhanil, E. Performance of self-healing gopolymer paste produced using bacillus substilis. *Constr. Build. Mater.* **2022**, *325*, 126837. [CrossRef]
23. Tanyildizi, H.; Ziada, M.; Uysal, M.; Gungor, N.D.; Coskun, A. Comparison of bacteria-based self-healing method in metakaolin geopolymer mortars. *Case Stud. Constr. Mater.* **2022**, *16*, e00895. [CrossRef]
24. Hammad, N.; El-Nemr, A.; Shaaban, I. Application of bacillus subtilis as a self-healing agent for alkali-activated slag (AAS). *Next Mater.* **2026**, *10*, 101466. [CrossRef]
25. Luhar, S.; Luhar, I.; Shaikh, F.U.A. Review on Performance Evaluation of Autonomous Healing of Geopolymer Composites. *Infrastructures* **2021**, *6*, 94. [CrossRef]
26. Zhao, D.; Li, K.; Li, Y.; Chen, X.; Fan, J.; Zhu, J. Self-healing behavior of fly ash/slag-based engineered geopolymer composites under external alkaline environments. *Case Stud. Constr. Mater.* **2024**, *21*, e03361.
27. Ozen, M.Y.; Firdous, R.; Lehmann, C.; Stephan, D. Autonomous self-healing behavior of geopolymer pastes under varied curing environments. *Constr. Build. Mater.* **2024**, *426*, 136099. [CrossRef]
28. Ulugol, H.; Gunal, M.F.; Yaman, I.O.; Yildrim, G.; Sahmaran, M. Effects of self-healing on the microstructure, transport, and electrical properties of 100% construcion-and demolition-waste-based geopolymer composites. *Cem. Concr. Compos.* **2021**, *121*, 104081. [CrossRef]
29. Choi, S.J.; Lee, J.I.; Kim, C.Y.; Yoon, J.H.; Kim, K.H. Self-healing performance and durability characteristics of self-healing mortar according to the composition ratio of cementitious material-based capsules. *J. Korea Concr. Inst.* **2024**, *36*, 591–602. [CrossRef]
30. *KS L 5105*; Testing Method for Compressive Strength of Hydraulic Cement Mortars. Korea Industrial Standards. Korean Standards & Certification Information Center: Seoul, Republic of Korea, 2007; 5p.
31. *KS F 2423*; Standard Test Method for Tensile Spliiting Strength of Concrete. Korea Industrial Standards. Korean Standards & Certification Information Center: Seoul, Republic of Korea, 2011.
32. *ASTM C 1202*; Standard Test Method for Electrical Indication of Concrete's Ability to Resist Chloride Ion Penetration. American Society for Testing and Materials: West Conshohocken, PA, USA, 2019.
33. Guinea, G.V.; El-Sayed, K.; Rocco, C.G.; Elices, M.; Planas, J. The effect of the bond between the matrix and the aggretgates on the cracking mechanism and fracture paramenters of concrete. *Cem. Concr. Res.* **2002**, *32*, 1961–1970. [CrossRef]
34. Cao, V.D.; Pilehavar, S.; Bring, C.S.; Szczotok, A.M.; Rodriquez, J.F.; Carmaon, M.; Manasir, N.A.; Kjonikesen, A.L. Microencapsulated phase chang materials for enhancing the thermal performance of Portland cement concrete and geopolymer concrete for passive building applications. *Energy Convers. Manag.* **2017**, *133*, 56–66. [CrossRef]
35. Korehong, W.; Sinsiri, T.; Jaturapitakkul, C. Effect of palm oil fuel ash fineness on packing effect and pozzolanic reaction of bleneded cement paste. *Procedia Eng.* **2011**, *14*, 361–369. [CrossRef]
36. Liu, Q.; Cheng, A.; Sun, C.; Chen, K.; Wang, Y.; Li, W. Effects of aggregate's type and orientation on stress concentration and crack propagation of modeled concrete applied a shear force. *J. Build. Eng.* **2024**, *95*, 110340. [CrossRef]
37. Kim, C.H.; Kim, N.W. Durability evaluation of precaste concrete using blast furnace slag and fly ash. *J. Korea Concr. Inst.* **2021**, *33*, 629–635. [CrossRef]
38. Kim, H.S.; Lee, C.H.; Ann, K.Y. Feasibility of ferronickel slag powder for cementitious binders in concrete mix. *Constr. Build. Mater.* **2019**, *207*, 693–705. [CrossRef]
39. Zhao, J.; Li, Z.; Wang, D.; Yan, P.; Luo, L.; Zhang, H.; Zhang, H.; Gu, X. Hydration superposition effect and mechanism of steel slag powder and granulated blast furnace slag powder. *Constr. Build. Mater.* **2023**, *366*, 130101. [CrossRef]
40. Zheng, H.; Duan, Y.; Li, M.; Hou, D.; Wang, P.; Chen, J.; Li, S. Reaction molecular dynamics study of calcium alumino-silicate hydate gel in the hydration deposition process at the calcium silicate hydrates inerface: The influence of Al/Si. *J. Build. Eng.* **2024**, *86*, 108823. [CrossRef]
41. Wang, H.; Wu, H.; Xing, Z.; Wang, R.; Dai, S. The Effect of Various SI/Al, Na/Al Molar Ratios and Free Water on Micromorphology and Macro-Sterngth of Metakaoing-Based Geopolymer. *Materials* **2021**, *14*, 3845.
42. Li, Z.; Zhang, W.; Wang, R.; Chen, F.; Jia, X.; Cong, P. Effects of Reacitve MgO on the Reaction Process of Geopolymer. *Materials* **2019**, *12*, 526.
43. Hai, R.; Guan, Q.; Zhang, X.; Yang, F.; Cui, L.; Liu, J. Effect of Waterglass on theHydration Process of Salg-Fly Ash-Based Geoplymer. *Materials* **2025**, *18*, 2450. [CrossRef]

44. Chaitanya, M.S.K.; Nagaraju, T.V.; Gadhirahu, L.V.K.R.; Madepalli, V.R.; Jampana, S.N.R. Strength and micro-structural performance of geopolymer concrete using highly burned rice husk ash. *Mater. Today Proc.* 2023, *in press*. [CrossRef]
45. Aalomayri, T.; Adesina, A.; Das, S. Influence of amorphous raw rice husk ash as precursor and curing condition on the performance of alkali activated cocrete. *Case Stud. Constr. Mater.* **2021**, *15*, e00777.

Disclaimer/Publisher's Note: The statements, opinions and data contained in all publications are solely those of the individual author(s) and contributor(s) and not of MDPI and/or the editor(s). MDPI and/or the editor(s) disclaim responsibility for any injury to people or property resulting from any ideas, methods, instructions or products referred to in the content.